POLITECNICO
MILANO 1863

SCUOLA DI INGEGNERIA INDUSTRIALE
E DELL'INFORMAZIONE

Executive Summary of the Thesis

Resonant inelastic x-ray scattering study of the double-chain superconducting cuprate $YBa_2Cu_4O_8$

Laurea Magistrale in Engineering Physics - Ingegneria Fisica

Author: Federico Pisani

Advisor: Prof. Giacomo C. Ghiringhelli

Co-advisor: Dr. Nicholas B. Brookes

Academic year: 2020-2021

---

1. Introduction

1.1. Cuprates

Cuprate superconductors were discovered in 1986 and from that moment on they have raised more and more interest. They possess a relatively high superconducting transition temperature with respect to standard superconductors. This is a very appealing property for potential applications as liquid nitrogen, instead of liquid helium, could be used in the cooling process, thus avoiding the high costs and technical complications involved with the use of the last. The common feature of all cuprate families is a layered structure which consists of CuO_2 planes. Between these planes other intermediate layers are located, which contain oxygen and one or more heavy atoms (such as Hg, Ba, or rare earths). In the CuO_2 planes, copper ions are nominally divalent (Cu^{2+}), i.e., they have a $3d^9$ electronic configuration. This means that each Cu, having a single unpaired electron, carries a spin 1/2. Each copper is surrounded by four in-plane oxygens. The superexchange interaction between Cu spins is crucial for the physics of cuprates. Superexchange is an indirect exchange interaction between non-neighbouring magnetic ions whose result is the stabilisation of an antiferromagnetic (AFM) ground state. One important consequence of Coulomb and superexchange interactions is the 2D nature of the electronic and magnetic physical properties in cuprates. The schematic representation of the direct and reciprocal bi-dimensional spaces is shown in Fig. 1 (a) and (b). Due to the AFM order, the nuclear and magnetic first Brillouin zones do not coincide.

Acting on the chemical composition of the intermediate layers or adding oxygen allow to control the number of electrons in the CuO_2 planes, i.e., to modify the doping level of the material. More precisely, the doping quantifies the extra-electrons or extra-holes per Cu atom. Hereafter, for the purpose of this summary, we will focus on hole-doped cuprates. Hole-doped cuprates exhibit a rich phase diagram: depending on temperature and doping level (p) many different phases arise. Hole doping quickly suppresses the antiferromagnetic order, making the superconducting (SC) state appear in the range $0.05 \leq p \leq 0.27$, below the Curie temperature T_C. Cuprates are unconventional superconductors where the pairing mechanism between charges shows a d-wave symmetry. The mech-

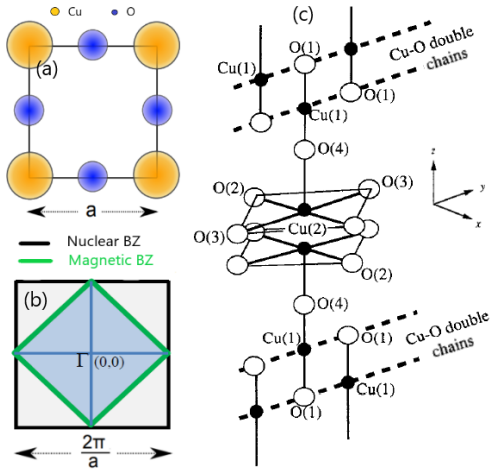

Figure 1: (a) and (b) represent the real and reciprocal spaces of a $Cu0_2$ lattice unit cell. (c) Schematic illustration of Y124 crystalline structure. Y and Ba atoms are not shown.

anism at the base of superconductivity is still not well-understood in high-temperature superconductors, such as cuprates, but many theories consider magnetic excitations as the possible acting force that drives the pairing mechanism. Indeed, although the long-range AFM order is destroyed in the SC phase, spins have still the possibility of creating local arrangements of magnetic moments if the exchange length is large enough.

Charge order phase can arise at doping levels similar to those where SC is present. Charge order indicates a phase where charges self-organise into superlattice structures. The high-electronic correlation which characterises cuprate systems could be the driving mechanism behind the appearance of charge order. When charge order takes the shape of a periodical modulation of valence charges, typically with unidirectional character, is usually referred to as charge density waves (CDWs). Charge order was essentially observed in all cuprate families, even though specific details vary from system to system. For instance, in lanthanum-based cuprates stripe-like CDWs appear with a periodicity which is a multiple of the underlying crystalline lattice periodicity, whereas in the Y123 family ($YBa_2Cu_3O_{6+x}$) incommensurate bi-axial CDWs were observed. Let us point out that the arising of the SC phase suppresses charge order, indicating a clear competition between these two phases.

1.2. $YBa_2Cu_4O_8$

The main focus of this thesis has been the investigation of the presence of charge density waves in $YBa_2Cu_4O_8$ (Y124). Y124 is the only cuprate which possesses a clean stoichiometry at all temperatures, with a highly robust oxygen content. Thus, it represents a unique opportunity to measure a defect-free cuprate system. Y124 possesses a base-centered-orthorombic structure with lattice constants

$$a = 3.84\,\text{Å}, \quad b = 3.87\,\text{Å}, \quad c = 27.23\,\text{Å} \qquad (1)$$

A schematic illustration of the Y124 crystalline structure is depicted in Fig. 1 (c). One major structural difference from Y123, which is a single-chain system, is the presence of Cu-O double chains.

Quantum oscillation (QO) experiments allow to map the Fermi surface of metals under the application of a strong magnetic field. $YBa_2Cu_3O_{6.5}$ and Y124 display similar quantum oscillation frequencies, indicating that similar Fermi surface reconstruction occurs in both compounds, which was suggested to involve CDW formation [1]. The missed observation of CDWs in the first work on this compound by Ghiringhelli *et al.* [2] may be due to several reasons, such as a weak signal, a non-optimised alignment or other experimental details. All these thoughts lay the foundations for this investigation.

The Y124 samples we measured are high-quality untwinned single crystals grown by the "Crystal Growth" group at Max Planck Institute for solid state research (Stuttgart, Germany) and are characterised by $p \sim 0.14$ and T_C around 80 K.

2. Methods

2.1. Resonant inelastic x-ray scattering

Resonant inelastic x-ray scattering (RIXS) is a photon-in photon-out spectroscopy which allows to study several intrinsic excitations of the material under study. An illustration of the process from the initial state to the final one can be visualised in Fig. 2. As a starting point, we can consider a photon characterised by a certain energy E and momentum $\mathbf{k}$. Since E is chosen such that it resonates with an atomic transition, the cross section of the process is strongly enhanced.

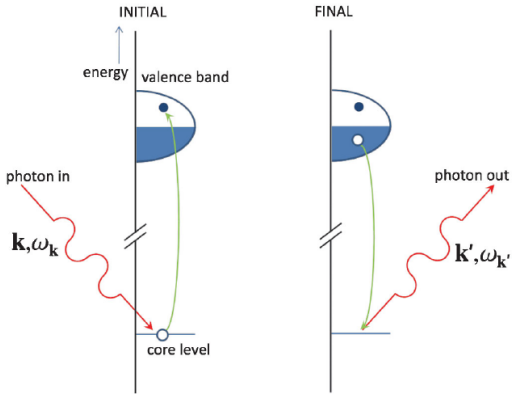

Figure 2: Phases of the RIXS process. The incoming photon promotes a core-level electron up to the valence band. A few fs later, a valence band electron decays and fills the core hole. This process results in the emission of a photon.

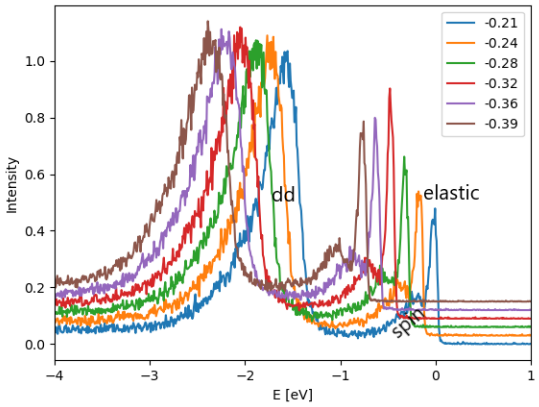

Figure 3: Selected RIXS spectra at different K values. The elastic line, the magnetic excitations ("spin") and the interorbital (dd) excitations are indicated.

When the photon impinges on the system, it interacts with an atom and causes the transition of a core electron up to the valence band. The atom finds itself in an excited state whose lifetime is typically very short, approx. 1 fs–2 fs. This is clearly an unstable condition. In order to reduce the overall energy of the ion, an electron from the valence band decays filling the core hole back. This can come with a radiative decay, where a photon is emitted with energy E' and momentum **k'**. If the difference $\Delta E = E - E'$ is non-zero, this means that some sort of excitation has been created in the system. The excitation is also characterised by momentum $\mathbf{q} = \mathbf{k} - \mathbf{k'}$. However, since the main physics of cuprates occurs in the CuO_2 planes, the relevant quantity for us is just the momentum in-plane component $\mathbf{q}_{\parallel}$.

RIXS has several advantages, including that it requires just small sample volumes and, in the case of cuprates and of the Cu L_3 edge, it allows for the investigation of a significant portion of the reciprocal lattice space. RIXS can probe a wide class of intrinsic excitations including charge transfer and dd (intraband) excitations in strongly correlated materials and lattice excitations. Moreover, magnetic excitations are also symmetry allowed in RIXS since the impinging photon carries angular momentum and this can be transferred to the electron spin angular momentum in the scattering process.

We performed our measurements at the ID32 beamline of the European Synchrotron (ESRF), which houses a pioneering high-resolution RIXS setup. The sample orientation in the beam can be fully controlled through a 4-circle in-vacuum goniometer. By gradually varying the scattering geometry it is possible to map the spectral features in momentum space. We conducted the experiments in grazing incidence geometry with the outgoing beam near the normal to the surface, corresponding to negative values for the Miller indices H and K related to the $\mathbf{q}_{\parallel}$.

3. Results

3.1. Charge density waves in Y124

We performed RIXS at the Cu L_3 edge ($E \approx 931.4$ eV) on high-quality Y124 single crystals at $T_C = 80$ K. Spectra were collected with a combined instrumental resolution of approx 65 meV and we used vertical (σ) polarisation to maximise the RIXS signal coming from charge ordering phenomena. Fig. 3 shows RIXS spectra collected at different K values. Three major features can be identified in each spectrum. The quasielastic peak corresponds to the range $[-0.1, 0.1]$ eV of energy loss. It derives from elastic scattering events, but it also includes the contribution coming from low-energy excitations such as phonons. The spectral feature which corresponds to the magnetic excitations is marked by the label "spin". The last evident spectral feature is related to the dd (intraband) excitations, which are the result of electronic transitions between different $3d$ states. Focusing on the quasielastic peak we observed that its am-

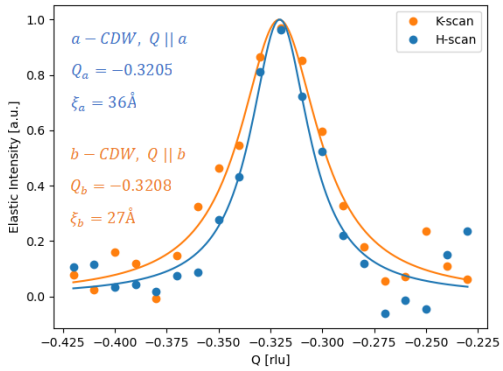

Figure 4: H- and K-scans collected at T_C. Lines are the fitted Lorentzian profile. Correlation lengths (ξ) and momentum position for both peaks are given.

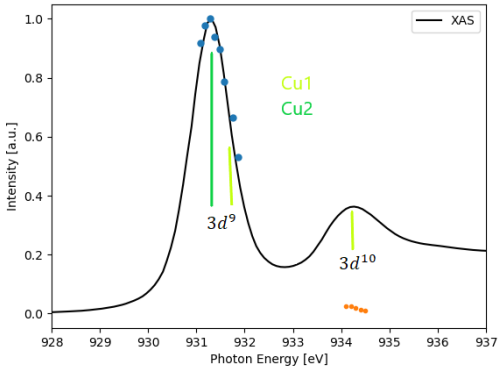

Figure 5: The black line corresponds to the XAS, whereas blue and orange points show the energy dependence of the CDW signal. XAS and RIXS data have been collected at room temperature and 80 K, respectively, and have been normalised. Cu1 and Cu2 label copper atoms in CuO chain layers and CuO_2 planes, respectively. Vertical bars indicate relevant absorption peaks.

plitude changes as a function of K, reaching a maximum at $K = -0.32\,\mathrm{r\,l\,u}$. We fitted the quasielastic intensities as a function of momentum with a Lorentizan profile on top of a linear background. We decided to employ a linear background since it nicely matches the edges of each scan and also because the scans collected at high temperatures (above 200 K) are linear signals without any recognizable peaks. Fig. 4 displays the result after background subtraction. A K-scan corresponds to a configuration in which the σ polarisation of the incoming x-ray beam is oriented perpendicular to the Y124 chains, whereas for an H-scan the σ polarisation is parallel to the Y124 chains. Along both H- and K-directions, it is possible to observe a clear peak, ascribable to a static elastic scattering due to the modulation of the valence charge. Additionally, the characteristic momenta for CDWs along the two directions, H_{CDW} and K_{CDW}, share the same value around $-0.32\,\mathrm{r\,l\,u}$. What is important to notice is that the a- and b-CDW peaks in reciprocal space in Y124 samples are very similar to those observed in Y123 [3]. This means that the a- and b-CDW domains in real space are also similar.

We measured the energy dependence of the CDW signal together with Y124 x-ray absorption spectroscopy (XAS). They are reported in Fig. 5. Two separated peaks are identifiable in the XAS. The first peak lies at energy around 933.2 eV, in correspondence of the Cu1 $3d^{10}$ configuration. It confirms that this is the electronic configuration for copper atoms in Y124 chains. The second peak lies at $E \approx 931.4\,\mathrm{eV}$ and it is associated with the Cu2 $3d^9$ configuration of the copper atoms belonging to the CuO_2 planes. Considering the energy profile of the RIXS quasielastic intensities (points in Fig. 5), it shows an enhancement at the energy of planar coppers, whereas a suppression is present at the energy of chain Cu. The direct conclusion is that charge order must be only connected to the modulation of planar coppers' valence electrons.

We then focused on the temperature dependence of the CDW signal. We observed that a peak is present for temperatures both below and above T_C, indicating the existence of CDWs for a wide temperature range. The peak seems to decrease in intensity (with respect to the background) and to broaden upon warming, until it is not recognisable anymore above $T = 200\,\mathrm{K}$. Since no evidence of CDWs is present at 200K or above, we can consider as onset temperature for charge order in Y124 the value $T_{CDW} \approx 190K$. After subtracting the background, we plotted the temperature dependence of the quasielastic peak intensity in Fig. 6 (a). Data show a concave-downward which resembles an order parameter of broken symmetry. Thus, we decided to use the power law of an order parameter to fit the data points.

$$I \propto (order\ parameter)^2 \propto (T_{CDW} - T)^{2\beta} \quad (2)$$

The good agreement between data and power law fit (shown in the same figure) strongly sug-

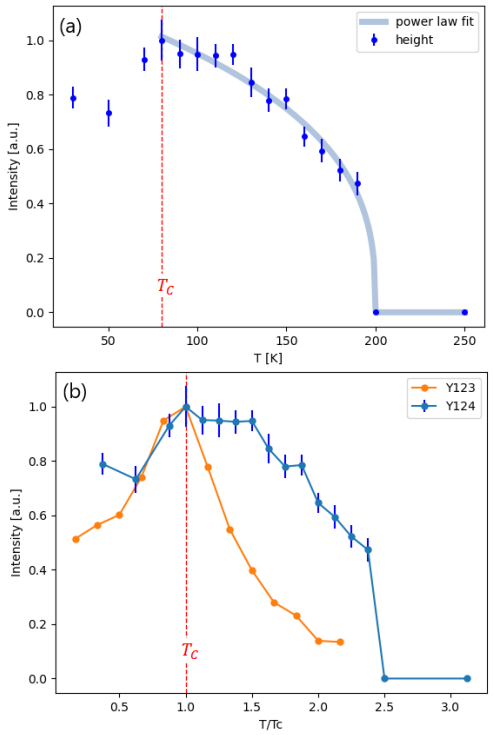

Figure 6: (a) Temperature dependence of the CDW peak height. Error bars, which represent a standard deviation of the fitting parameter, are also indicated. The blue curve is the result of the power law fitting. (b) Comparison between temperature dependence in Y124 and Y123 compounds. Data have been normalised according to their critical temperature ($T_C(Y123) \approx 60\,\mathrm{K}$). Y123 points have been extrapolated from Ref. [3].

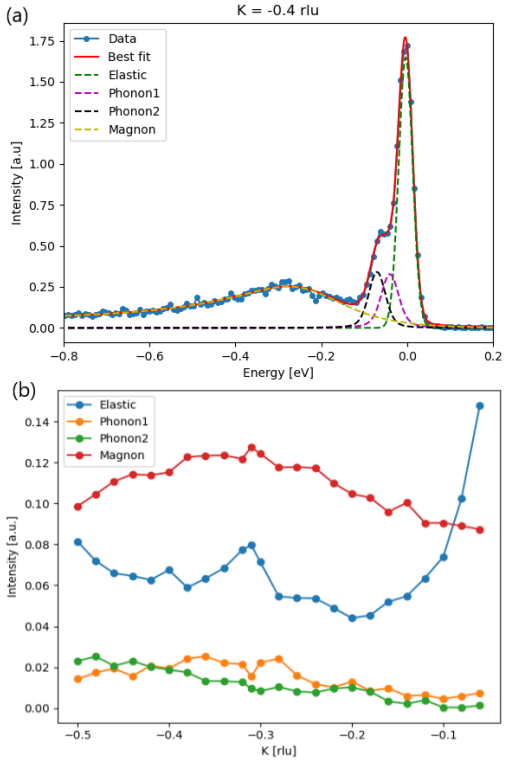

Figure 7: (a) Data fitting of the RIXS spectrum collected at $K = -0.40\,\mathrm{r\,l\,u}$. The best fit is indicated by the red line, whereas each dashed line represents one specific spectral feature. (b) Momentum dependence of the intensity related to each spectral feature.

gests that the clean stoichiometry of Y124 allows CDWs to develop as a true second order phase transition. To make a comparison with the related Y123 compound, Fig. 6 (b) reports our results together with the data by Blanco-Canosa *et al.* [3] collected on $YBa_2Cu_3O_{6.6}$ (Y123). Both data sets are peaked at the critical temperature, but the temperature dependence exhibited by Y124 is markedly different from that of Y123, especially above T_C. One possible explanation for this discrepancy could be attributed to the oxygen stability which characterises the Y124 compound in contrast with Y123, which carries intrinsic stoichiometric defects associated with the oxygen content in the CuO chain layers. Below T_C, the CDW signal is suppressed similarly in the two data sets, reconfirming the competition between charge order and superconductivity.

3.2. Phonons and magnetic excitations

We collected RIXS spectra with high-energy resolution ($\Delta E \approx 35\,\mathrm{meV}$) at $T_C = 80\,\mathrm{K}$. They allowed us to study the dispersions of the inelastic RIXS features in detail. This was possible by fitting the data with the sum of different functions, each of them representing a specific feature of the RIXS spectrum. Fig. 7 (a) reports, as an example, the data fitting on a selected RIXS spectrum. The elastic peak is fitted with a Gaussian profile centred around zero. Its FWHM has been fixed to the width of the combined experimental resolution of beamline and spectrometer. Concerning phonons, RIXS is able to probe two main vibrational modes in cuprates. They are the buckling mode, which consists in the vibration of planar oxygen atoms out of the CuO_2 planes, and the breathing mode, related to the stretching of Cu-O bonds. They lie at energies around 35 meV and 70 meV, respectively. Two Voigt profiles have been used to fit them ("phonon 1" and "phonon2" label the

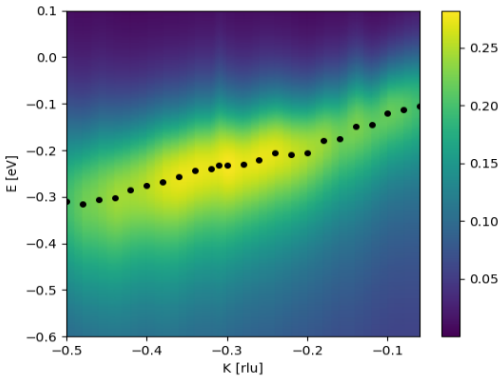

Figure 8: Intensity colormap of the magnetic excitations. Black points are related to the position of the paramagnon peak and give an idea of the magnetic dispersion.

buckling mode and the breathing mode, respectively). Lastly, to model the asymmetric shape of the magnetic feature, we decided to employ the Fano lineshape, which turns out to be a suitable fit for the shape of the magnetic peak. Fig. 7 (b) shows the K dependence of each spectral feature. For the elastic contribution is again recognisable the CDW peak. Phonon 1 shows an enhancement of the intensity in the central momentum region, where CDW arises. Therefore, it gives a contribution to the quasielastic intensity peak at K_{CDW}. Instead, phonon 2 is characterised by a decreasing trend when moving from $-0.50\,\mathrm{r\,l\,u}$ to $-0.06\,\mathrm{r\,l\,u}$. The coupling between phonons and electrons is a consequence of the lattice deformation: the kinetic energy of electrons is modified since lattice vibrations change the way in which orbitals of nearby ions overlap. Since the larger the momentum, the shorter the spatial periodicity of the lattice vibrations, a more pronounced deformation of the lattice and a stronger electron-phonon coupling take place at larger $|K|$. The enhancement in intensity when moving towards higher $|K|$ values is evident and our results are in good agreement with predictions derived from an 8-band Cu-O model [4].

Considering magnetic excitations, we tracked their dispersion in the reciprocal space. As the Y124 doping level places it far away from the antiferromagnetic phase, we are dealing with damped spin-waves, i.e., paramagnons in a quantum picture. The paramagnon dispersion is highlighted by black points in the colormap of Fig. 8. Differently from data reported by Le Tacon *et al.* [5] on Y124, which show an energy at the Brillouin zone boundary of around 225 meV, our results seem to confirm an energy at the BZ boundary of ≈ 300 meV, similarly to other cuprate systems. This discrepancy can be due to the better quality of the Y124 crystals and the absence of multidomain configurations in our samples.

4. Conclusions

We used Cu L_3 edge RIXS on high-quality untwinned Y124 single crystals to investigate the presence of charge density waves (CDWs). Indeed, we observed a peak in the quasielastic intensity which is ascribable to a charge order phase. The peak is centred at a similar momentum value as observed in other cuprate families, such as $YBa_2Cu_3O_{6+x}$ (Y123). Furthermore, the presence of the CDW signal was confirmed along both the in-plane directions of the reciprocal space, with unidirectional domains similar in shape and size to those observed in YBCO. By studying the energy dependence of the CDW signal, we came to the conclusion that charge order is associated with the valence electrons of the CuO_2 planes' copper atoms alone. We also considered the temperature evolution of the CDW signal in Y124. At high temperatures, it shows a trend comparable to an order parameter of broken symmetry. We attributed this behaviour to the clean stoichiometry which characterises Y124. This defect-free scenario should allow the CDWs to fully develop as a second order phase transition.

We collected RIXS spectra with high-resolution, around 35 meV. They allowed us to conduct a detailed study of the dispersions of the inelastic RIXS features in the reciprocal space. We focused on the spin collective modes which arise from planar Cu atoms, tracking their dispersion in the reciprocal space. We observed that they are characterised by an energy value around 300 meV at the edge of the first Brillouin zone, in analogy to other cuprate materials.

Our findings demonstrates that CDWs are present in the Y124 system and give an outlook about the correlation between disorder and charge ordering phenomena. Our results will inform future investigations and theoretical models of charge and spin collective phenomena in high-T_C cuprate superconductors and akin

quantum materials.

5. Acknowledgements

I thank the ESRF for the allocation of synchrotron radiation beamtime and the "Crystal Growth" group of Max Planck Institute for solid state research (Stuttgart, Germany) for providing the samples. I would like to express my gratitude to Prof. Giacomo Ghiringhelli, which let me get in touch with this stunning opportunity. A special thank go to all the members of the ID32 beamline at the ESRF.

References

[1] E. A. Yelland et al. Quantum Oscillations in the Underdoped Cuprate $YBa_2Cu_4O_8$. *Phys. Rev. Lett.*, 100, 2008.

[2] G. Ghiringhelli et al. Long-Range Incommensurate Charge Fluctuations in (Y,Nd)$Ba_2Cu_3O_{6+x}$. *Science*, 337, 2012.

[3] S. Blanco-Canosa et al. Resonant x-ray scattering study of charge-density wave correlations in $YBa_2Cu_3O_{6+x}$. *Phys. Rev. B*, 90, 2014.

[4] T. P. Devereaux et al. Directly Characterizing the Relative Strength and Momentum Dependence of Electron-Phonon Coupling Using Resonant Inelastic X-Ray Scattering. *Phys. Rev. X*, 6, 2016.

[5] M. Le Tacon et al. Intense paramagnon excitations in a large family of high-temperature superconductors. *Nature Physics*, 7, 2011.